IEEE TRANSACTIONS ON
INDUSTRIAL ELECTRONICS

MAY 2015 VOLUME 62 NUMBER 5 ITIED6 (ISSN 0278-0046)

PAPERS

Multiphase Systems

Enhanced DC-Link Capacitor Voltage Balancing Control of DC–AC Multilevel Multileg Converters . . . . . *S. Busquets-Monge, R. Maheshwari, J. Nicolas-Apruzzese, E. Lupon, S. Munk-Nielsen, and J. Bordonau* 2663

A Simple Approach to Damp SSR in Series-Compensated Systems via Reshaping the Output Admittance of a Nearby VSC-Based System . . . . . *K. M. Alawasa and Y. A.-R. I. Mohamed* 2673

An Enhanced Voltage Sag Compensation Scheme for Dynamic Voltage Restorer . . . . . *A. M. Rauf and V. Khadkikar* 2683

Predictive Voltage Control of Transformerless Dynamic Voltage Restorer . . . . . *C. Kumar and M. K. Mishra* 2693

On Dynamic Models and Stability Analysis of Three-Phase Phasor PWM-Based CSI for Stand-Alone Applications . . . . . *A. Singh, A. K. Kaviani, and B. Mirafzal* 2698

Current Harmonics Compensation Based on Multiresonant Control in Synchronous Frames for Symmetrical n-Phase Machines . . . . . *A. G. Yepes, J. Malvar, A. Vidal, O. López, and J. Doval-Gandoy* 2708

Machines and Drive

Analysis and Comparison of Peak-to-Peak Current Ripple in Two-Level and Multilevel PWM Inverters . . . . . *G. Grandi, J. Loncarski, and O. Dordevic* 2721

Predictive Torque Control of a Multidrive System Fed by a Dual Indirect Matrix Converter . . . . . *M. López, J. Rodriguez, C. Silva, and M. Rivera* 2731

Analytical Calculation of the Slot Leakage Inductance in Fractional-Slot Concentrated-Winding Machines . . . . . *B. Prieto, M. Martínez-Iturralde, L. Fontán, and I. Elosegui* 2742

Speed Measurement Error Suppression for PMSM Control System Using Self-Adaption Kalman Observer . . . . . *T. Shi, Z. Wang, and C. Xia* 2753

Single-Phase Electronics

Energy Sharing Control Scheme for State-of-Charge Balancing of Distributed Battery Energy Storage System . . . . . *W. Huang and J. A. Abu Qahouq* 2764

Decentralized Voltage-Sharing Control Strategy for Fully Modular Input-Series–Output-Series System With Improved Voltage Regulation . . . . . *W. Chen and G. Wang* 2777

Calculation of Temperature Field in Power Capacitor . . . . . *Y. Liang, D. Wang, L. Gao, and D. Liu* 2788

ZCS Bridgeless Boost PFC Rectifier Using Only Two Active Switches . . . . . *K. S. B. Muhammad and D. D.-C. Lu* 2795

Analysis of Capacitive Impedance Matching Networks for Simultaneous Wireless Power Transfer to Multiple Devices . . . . . *J. Kim, D.-H. Kim, and Y.-J. Park* 2807

Shielding-Cancelation Technique for Suppressing Common-Mode EMI in Isolated Power Converters . . . . . *L. Xie, X. Ruan, Q. Ji, and Z. Ye* 2814

(Contents Continued on Page 2661)

A PUBLICATION OF THE IEEE INDUSTRIAL ELECTRONICS SOCIETY

(Contents Continued from Front Cover)

Renewable Energy Systems

Predictive Control With Novel Virtual-Flux Estimation for Back-to-Back Power Converters . . . . . *Z. Zhang, H. Xu, M. Xue, Z. Chen, T. Sun, R. Kennel, and C. M. Hackl* 2823

Voltage-Balancing Method for Modular Multilevel Converters Switched at Grid Frequency . . . . . *F. Deng and Z. Chen* 2835

A Novel Integrated Power Quality Controller for Microgrid . . . . . *D. Li and Z. Q. Zhu* 2848

A Modular Multilevel Converter Pulse Generation and Capacitor Voltage Balance Method Optimized for FPGA Implementation . . . . . *W. Li, L.-A. Grégoire, and J. Bélanger* 2859

High-Voltage Tapped-Inductor Buck Converter Utilizing an Autonomous High-Side Switch . . . . . *T. Modeer, S. Norrga, and H.-P. Nee* 2868

Multilevel Modular DC/DC Power Converter for High-Voltage DC-Connected Offshore Wind Energy Applications . . . . . *A. Parastar, Y. C. Kang, and J.-K. Seok* 2879

Robotics and Mechatronics

Nonlinear Robust Adaptive Tracking Control of a Quadrotor UAV Via Immersion and Invariance Methodology . . . . . *B. Zhao, B. Xian, Y. Zhang, and X. Zhang* 2891

Cost-Efficient Integration of Industrial Applications Using Smart Power Gate Arrays . . . . . *Y. Zhang, C. Scherjon, and J. N. Burghartz* 2903

A Recursive Receding Horizon Planning for Unmanned Vehicles . . . . . *B. Zhang, L. Tang, J. DeCastro, M. J. Roemer, and K. Goebel* 2912

Calibration-Based Iterative Learning Control for Path Tracking of Industrial Robots . . . . . *Y. M. Zhao, Y. Lin, F. Xi, and S. Guo* 2921

Control and Signal Processing

Data-Driven Optimization Control for Safety Operation of Hematite Grinding Process . . . . . *W. Dai, T. Chai, and S. X. Yang* 2930

The Active Control of Maglev Stationary Self-Excited Vibration With a Virtual Energy Harvester . . . . . *J. Li, J. Li, D. Zhou, P. Cui, L. Wang, and P. Yu* 2942

Embedded Systems

Architecture of FPGA Embedded Multiprocessor Programmable Controller . . . . . *Z. Hajduk, B. Trybus, and J. Sadolewski* 2952

Intelligent Systems

An Advanced Single-Image Visibility Restoration Algorithm for Real-World Hazy Scenes . . . . . *S.-C. Huang, J.-H. Ye, and B.-H. Chen* 2962

An Affine-Arithmetic-Based Consensus Protocol for Smart-Grid Computing in the Presence of Data Uncertainties . . . . . *V. Loia, V. Terzija, A. Vaccaro, and P. Wall* 2973

A PSO-Based Fuzzy-Controlled Searching for the Optimal Charge Pattern of Li-Ion Batteries . . . . . *S.-C. Wang and Y.-H. Liu* 2983

Networking

When Scavengers Meet Industrial Wireless . . . . . *B. Martinez, X. Vilajosana, F. Chraim, I. Vilajosana, and K. S. J. Pister* 2994

Localization Bias Reduction in Wireless Sensor Networks . . . . . *Y. Ji, C. Yu, J. Wei, and B. Anderson* 3004

SPECIAL SECTION ON INDUSTRIAL ELECTRONICS FOR ELECTRIC TRANSPORTATION

Industrial Electronics for Electric Transportation . . . . . *S. S. Williamson, A. K. Rathore, and F. Musavi* 3017

Industrial Electronics for Electric Transportation: Current State-of-the-Art and Future Challenges . . . . . *S. S. Williamson, A. K. Rathore, and F. Musavi* 3021

A Single-Phase Active Device for Power Quality Improvement of Electrified Transportation . . . . . *A. Javadi and K. Al-Haddad* 3033

Large-Signal Characterization of Power Inductors in EV Bidirectional DC–DC Converters Focused on Core Size Optimization . . . . . *M. S. Perdigão, J. P. F. Trovão, J. M. Alonso, and E. S. Saraiva* 3042

Power Electronics Control of an Energy Regenerative Mechatronic Damper . . . . . *Y. M. Roshan, A. Maravandi, and M. Moallem* 3052

(Contents Continued on Page 2662)

(Contents Continued from Page 2661)

Position-Based T-S Fuzzy Power Management for Tram With Energy Storage System . . . . . J. Talla, L. Streit, Z. Peroutka, and P. Drabek 3061
Loss and Efficiency Analysis of Switched Reluctance Machines Using a New Calculation Method . . . . . Q. Yu, B. Bilgin, and A. Emadi 3072
Power Quality Issues in Railway Electrification: A Comprehensive Perspective . . . . . S. M. Mousavi Gazafrudi, A. Tabakhpour Langerudy, E. F. Fuchs, and K. Al-Haddad 3081
Self-Excited Induction Generator as an Auxiliary Brake for Heavy Vehicles and Its Analog Controller . . . . . J.-N. Bae, Y.-E. Kim, Y.-W. Son, H.-S. Moon, C.-H. Yoo, and J. Lee 3091
Potential of Using Multiterminal LVDC to Improve Plug-In Electric Vehicle Integration in an Existing Distribution Network . . . . . W. Pei, W. Deng, X. Zhang, H. Qu, and K. Sheng 3101
Model-Based Virtual Thermal Sensors for Lithium-Ion Battery in EV Applications . . . . . Y. Xiao 3112
Investigating Wireless Charging and Mobility of Electric Vehicles on Electricity Market . . . . . C.-H. Ou, H. Liang, and W. Zhuang 3123
Modeling and Analyzing Multiport Isolation Transformer Capacitive Components for Onboard Vehicular Power Conditioners . . . . . B. Farhangi and H. A. Toliyat 3134
Sensorless SVPWM-FADTC of a New Flux-Modulated Permanent-Magnet Wheel Motor Based on a Wide-Speed Sliding Mode Observer . . . . . Y. Fan, L. Zhang, M. Cheng, and K. T. Chau 3143
A Zero-Voltage-Transition Bidirectional DC/DC Converter . . . . . S. Dusmez, A. Khaligh, and A. Hasanzadeh 3152
Novel Modular Multiple-Input Bidirectional DC–DC Power Converter (MIPC) for HEV/FCV Application . . . . . A. Hintz, U. R. Prasanna, and K. Rajashekara 3163
Dynamic Performance Improvement and Peak Power Limiting Using Ultracapacitor Storage System for Hydraulic Mining Shovels . . . . . O. Abdel-baqi, A. Nasiri, and P. Miller 3173
SiC Integrated Circuit Control Electronics for High-Temperature Operation . . . . . M. Alexandru, V. Banu, X. Jordà, J. Montserrat, M. Vellvehi, D. Tournier, J. Millán, and P. Godignon 3182
Improved Stability of DC Catenary Fed Traction Drives Using Two-Stage Predictive Control . . . . . V. Šmídl, Š. Janouš, and Z. Peroutka 3192
Four-Axis Vector-Controlled Dual-Rotor PMSM for Plug-in Electric Vehicles . . . . . A. V. Sant, V. Khadkikar, W. Xiao, and H. H. Zeineldin 3202
A Modular Multiport Power Electronic Transformer With Integrated Split Battery Energy Storage for Versatile Ultrafast EV Charging Stations . . . . . M. Vasiladiotis and A. Rufer 3213
A Real-Time Energy Management Architecture for Multisource Electric Vehicles . . . . . J. P. F. Trovão, V. D. N. Santos, C. H. Antunes, P. G. Pereirinha, and H. M. Jorge 3223
Investigation of Permanent-Magnet Motor Drives Incorporating Damper Bars for Electrified Vehicles . . . . . X. Lu, K. L. V. Iyer, K. Mukherjee, K. Ramkumar, and N. C. Kar 3234
Model-Based Range Extension Control System for Electric Vehicles With Front and Rear Driving–Braking Force Distributions . . . . . H. Fujimoto and S. Harada 3245
An Improved Robust Field-Weakeaning Algorithm for Direct-Torque-Controlled Synchronous-Reluctance-Motor Drives . . . . . X. Zhang, G. H. B. Foo, D. M. Vilathgamuwa, and D. L. Maskell 3255
Phase Current Reconstruction of Switched Reluctance Motors From DC-Link Current Under Double High-Frequency Pulses Injection . . . . . C. Gan, J. Wu, S. Yang, and Y. Hu 3265
Design and Performance of a Cost-Effective BLDC Drive for Water Pump Application . . . . . M. Z. Youssef 3277
Onboard Integrated Battery Charger for EVs Using an Asymmetrical Nine-Phase Machine . . . . . I. Subotic, N. Bodo, E. Levi, and M. Jones 3285
DC–DC Converter for Dual-Voltage Automotive Systems Based on Bidirectional Hybrid Switched-Capacitor Architectures . . . . . D. Flores Cortez, G. Waltrich, J. Fraigneaud, H. Miranda, and I. Barbi 3296
Comparative Analysis of Bidirectional Three-Level DC–DC Converter for Automotive Applications . . . . . S. Dusmez, A. Hasanzadeh, and A. Khaligh 3305
Naturally Clamped Soft-Switching Current-Fed Three-Phase Bidirectional DC/DC Converter . . . . . P. Xuewei and A. K. Rathore 3316

Decentralized Voltage-Sharing Control Strategy for Fully Modular Input-Series–Output-Series System With Improved Voltage Regulation

Wu Chen, *Member, IEEE*, and Guangjiang Wang

***Abstract*—Input-series–output-series (ISOS) system connection of dc–dc converters is suitable for high-input–voltage and high-output-voltage applications. Input voltage sharing and output voltage sharing of the constituent modules among the ISOS system must be ensured. This paper proposes a novel decentralized voltage-sharing control strategy, which has the advantages of full modularity and high reliability, and each module is controlled independently without any control communication with other modules. In order to ensure proper sharing of input and output voltages, the input voltage sensing signal is added to the reference voltage for each module, resulting in the positive output voltage gradient regulation characteristic of the ISOS system; moreover, a system output voltage shifting loop is introduced to improve the system voltage regulation. The proposed control strategy can effectively improve the modularity and reliability of the ISOS system. An ISOS system prototype consisting of three two-transistor forward converter modules is tested in the laboratory, and the experimental results verify the effectiveness of the control strategy.**

***Index Terms*—Decentralized controller, input-series–output-series (ISOS), stability, voltage sharing, voltage shifting loop.**

I. Introduction

In high-voltage applications, the voltage stress of active switches in power converters is always a concern to power supply designers. Series connection of power switches is an advantageous solution; however, uneven voltage sharing among the series-connected devices, particularly during switching transient, cannot be avoided, and extra voltage balancing auxiliary circuits are required to overcome the problem [1]. The multilevel converter is a preferred choice to meet the high-voltage requirement with low-voltage low-power devices. In addition, series dc–dc power conversion system in which multiple standardized converter modules are connected in series at the input and/or output sides is also an alternative [2]–[5]. Due to the series connection of multiple modules, the ratings of the power devices in each single module are comparatively lower; moreover, reliability and maintainability of the power conversion system can be improved due to the redundancy provided by multiple modules.

For series-connection systems, input-series–output-parallel (ISOP) system, which consists of multiple modules connected in series at the input sides and in parallel at the output sides, is very well suited to high-input-voltage and large-output-current applications [6], whereas input-series–output-series (ISOS) system, consisting of multiple modules connected in series both at the input and output sides, is suitable for the applications where both input and output voltages are relatively high. For instance, the ISOS systems are expected to be employed in the power collection and transmission system to transmit the renewable energy to high-voltage dc grid [7].

It is critical to ensure equilibrium among the constituent modules for the proper operation of series-connection systems, i.e., input voltage sharing and output current sharing for the ISOP system and both input/output voltages sharing for the ISOS system. The equilibrium strategies for the ISOP system have been extensively studied [8]–[12], whereas only a few work have been done for the ISOS system. In [13], a three-loop control strategy composed of output voltage loop, inner current loop, and input voltage feedforward loop is proposed to achieve both input/output voltages sharing for the ISOS system. Although it is pointed out that the ISOS system with common duty ratio control scheme is unstable when there is even a very small mismatch in the turn rations of the transformers of the constituent modules [8], for some special circuit topologies, for instance, an ISOS system consisting of two full-bridge converters with the common duty ratio control scheme is stable due to the duty ratio loss characteristics of the full-bridge converter [14]. Merwe and Mouton [15] also identified that a weak natural rebalancing ability exists in the ISOS system with interleaved switching for different cells, and voltage dependent losses, such as the switching loss, enhance the rebalancing ability; however, the voltage-sharing performance is considerably affected by the load current. Reference [16] proposed an interesting idea called duty cycle exchanging control strategy, and it showed satisfactory results; however, the control strategy is merely effective to two-module ISOS system and cannot be used to the ISOS system consisting of three or more modules.

Manuscript received February 25, 2014; revised March 19, 2014, June 30, 2014, and August 8, 2014; accepted September 1, 2014. Date of publication October 28, 2014; date of current version April 8, 2015. This work was supported in part by the National Natural Science Foundation of China under Award 51307024, in part by the Research Fund for the Doctoral Program of Higher Education of China under Grant 20120092120053, in part by the Fundamental Research Funds for the Central Universities under Grant 2242014R30018, and in part by the Scientific Research Staring Foundation for the Returned Overseas Chinese Scholars, Ministry of Education of China.

The authors are with the Jiangsu Provincial Key Laboratory of Smart Grid Technology and Equipment, School of Electrical Engineering, Southeast University, Nanjing 210096, China (e-mail: chenwu@seu.edu.cn; 624240770@qq.com).

Color versions of one or more of the figures in this paper are available online at http://ieeexplore.ieee.org.

Digital Object Identifier 10.1109/TIE.2014.2365433

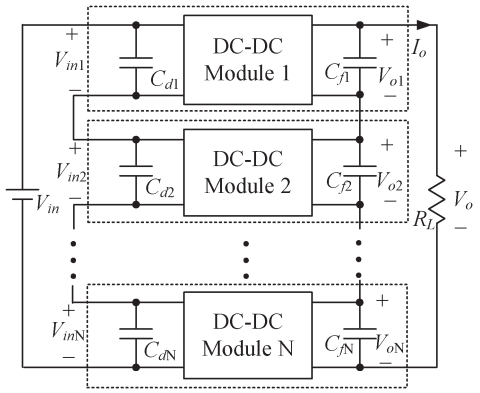

Fig. 1. Circuit diagram of an ISOS system.

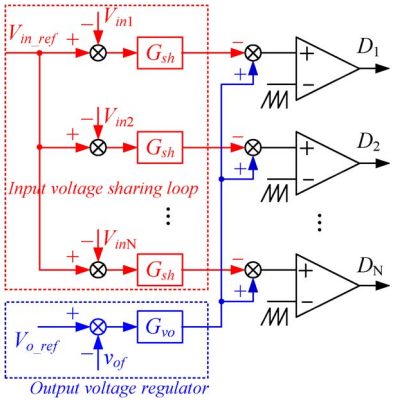

Fig. 2. Control strategy for the ISOS system in [4] and [13].

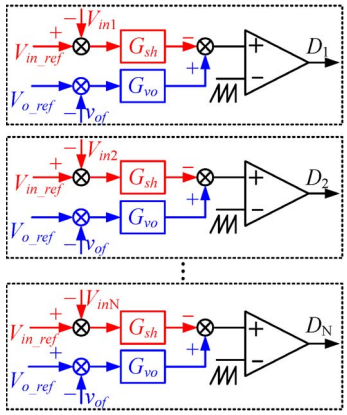

Fig. 3. OVR is dispatched to each module.

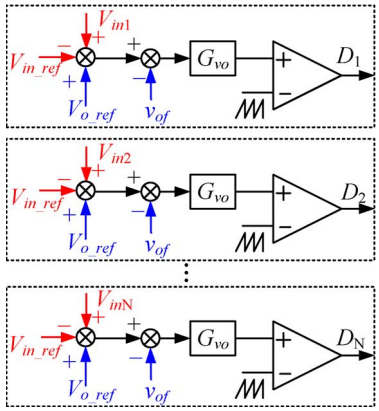

Fig. 4. Combination of the OVR and the IVSR.

For the ISOS systems with the aforementioned control strategies, all the constituent modules share the central controllers [13], [14], [16] or connected in master–slave mode [15], and the ISOS systems cannot accommodate the failures of the central controllers or the master module, resulting in lower redundancy and reliability of the system. Moreover, modularity and expansibility, which are the main benefits of the multimodule system, are also limited due to the central controllers.

In this paper, a decentralized voltage-sharing control strategy is proposed, with which fully modular architecture can be realized for the ISOS system. With the proposed control strategy, all the constituent modules are designed to be identical with the same power stages and control stages; in addition, the central controller is eliminated, and there is no any control interconnection among the modules, leading to superior system reliability and modularity.

II. Genesis of the Decentralized Voltage-Sharing Control Strategy

Fig. 1 illustrates the circuit diagram of an ISOS system consisting of N isolated dc–dc converter modules. For the ISOS system, a general control strategy was proposed to ensure both input/output voltages sharing in [4] and [13], as shown in Fig. 2. The control strategy consists of a system output voltage regulator (OVR) and N input voltage-sharing regulators (IVSRs). V_{o_ref} is the reference output voltage, v_{of} is the sampled system output voltage, G_{vo} is the compensation gain of OVR, G_{sh} is the gain of IVSR, and $V_{\mathrm{in\_ref}}$ is the reference voltage of each module input voltage, i.e.,

$$V_{\mathrm{in\_ref}} = \frac{V_{\mathrm{in1}} + V_{\mathrm{in2}} + \cdots + V_{\mathrm{in}N}}{N} = \frac{V_{\mathrm{in}}}{N}. \tag{1}$$

It can be seen that the drive signal of each module is composed of two parts: the output of OVR, which is common for all modules, and the output of each IVSR. In order to realize decentralized control, the OVR needs to be dispatched to each module, as shown in Fig. 3. It has been proved that the input voltage-sharing loop and the system output voltage loop are decoupled, and the OVR and the IVSR can be designed independently [4]. We arbitrarily design the OVR and the IVSR to have the same gain, and the control strategy can be redrawn as Fig. 4. In Fig. 4, there are four control signals for each module controller, i.e., V_{o_ref}, $V_{\mathrm{in}j}$ $(j = 1, 2, \ldots, N)$, v_{of}, and $V_{\mathrm{in\_ref}}$. V_{o_ref} is a constant given value. $V_{\mathrm{in}j}$ $(j = 1, 2, \ldots, N)$ is the module's own input voltage. v_{of} and $V_{\mathrm{in\_ref}}$ are two external input control signals. From the point of view of modularity, for the constituent module of the ISOS system, the less the external input control signals, the better the modularity and reliability. v_{of} is necessary to obtain the desired system output voltage. $V_{\mathrm{in\_ref}}$ is variable when the system input voltage varies, and if we set $V_{\mathrm{in\_ref}}$ as a constant value, such as $V_{\mathrm{in\,min}}/N$, then the external input control signal $V_{\mathrm{in\_ref}}$ is eliminated, and for each module, there is only one external input control signal

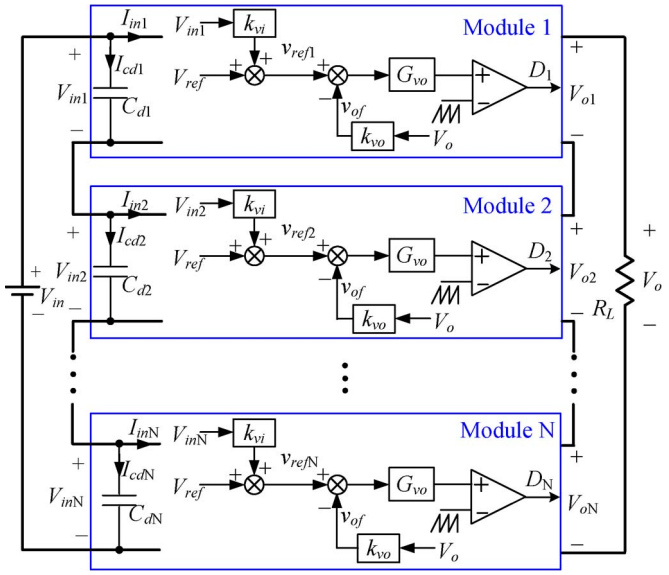

Fig. 5. Proposed decentralized voltage-sharing control strategy.

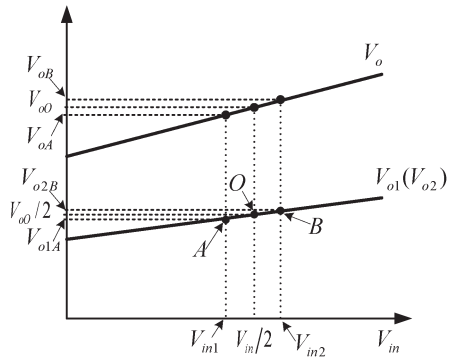

Fig. 6. Positive output voltage gradient regulation characteristics.

$v_{\rm of}$. The input voltage of each module varies in a certain range from $V_{\rm in\,min}/N$ to $V_{\rm in\,max}/N$. When the module input voltage increases from $V_{\rm in\,min}/N$, the error $V_{{\rm in}j} - V_{\rm in\_ref}$ $(j = 1, 2, \ldots, N)$ slowly increases from zero because $V_{\rm in\_ref}$ is set to be $V_{\rm in\,min}/N$, and the system output voltage slowly increases, too. Of course, $V_{\rm in\_ref}$ can be also set as a certain value between $V_{\rm in\,min}/N$ to $V_{\rm in\,max}/N$, which only affects the start position of the positive output voltage gradient regulation characteristics shown in Fig. 6. Then, the final configuration of the proposed control strategy is obtained, as illustrated in Fig. 5, where $k_{\rm vi}$ is the sensing factor of the module input voltage, $k_{\rm vo}$ is the sensing factor of the system output voltage, and $V_{\rm ref}$ is the combination of $V_{o\_\rm ref}$ and $V_{\rm in\_ref}$. The detailed control diagram block of the proposed control strategy is shown in Fig. 14, where V_{c1} represents the input reference $V_{\rm in\_ref}$ (set as a constant value). It is equal to the sampled value of the module minimum input voltage. V_{c1} is subtracted from the sampled signal of the module input voltage, which is not illustrated in Fig. 5.

Compared with Figs. 2 and 3, as $V_{\rm in\_ref}$ is set as a constant value, the external input control signal $V_{\rm in\_ref}$ can be directly designed in the control stage, and there is no need to sample the module input voltage through voltage transducers in Fig. 5. In other words, N control signal lines, which are easily disturbed by high-voltage and high-current parts, are removed from the ISOS system. From the point of view of modularity, the less the external input control signals and communication lines, the better the modularity and reliability. Therefore, the ISOS system with the proposed decentralized voltage-sharing control strategy shown in Fig. 5 has superior modularity and reliability compared with the existing control strategies.

III. Operation Principle of the Proposed Control Strategy

Fig. 5 shows the proposed decentralized voltage-sharing control strategy for the ISOS system. As shown, all the modules are designed to be the same, the controllers are distributed into each module, and there is no central controller. For each module, only the module input voltage and the system output voltage are sampled, and there is no other control signal communication among the modules. There is an output voltage loop in each single module, and the sampled signal of the module input voltage is added to the reference $V_{\rm ref}$, which is the difference from the conventional output voltage loop with constant reference and is the key part of the decentralized control strategy contributing to the voltage sharing. It can be seen that, for each module, the real reference $v_{{\rm ref}j}$ $(j = 1, 2, \ldots, N)$ increases with the increase in module input voltage, leading to the increase in the system output voltage; hence, the ISOS system with the proposed control strategy has positive output voltage gradient regulation characteristics, as shown in Fig. 6.

To simplify the analysis, a two-module ISOS system is taken as an example to explain the operation principle of the proposed control strategy. It is assumed that the two modules have the same output voltage regulation characteristics, as shown in Fig. 6. At steady state, the two modules share the input/output voltage, and both work at point O, i.e., $V_{\rm in1} = V_{\rm in2} = V_{\rm in}/2$, and $V_{o1} = V_{o2} = V_{oO}/2$. Assuming that a perturbation occurs on the input divided capacitor voltages, e.g., $V_{\rm in1}$ decreases and $V_{\rm in2}$ increases, i.e., $V_{\rm in1} < V_{\rm in}/2 < V_{\rm in2}$, whereas the input voltage $V_{\rm in}$ is unchanged. From Fig. 5, it can be seen that, although system output voltage V_o is taken as the feedback signal for each module controller, only the module's own output voltages V_{oj} $(j = 1, 2, \ldots, N)$ can be directly controlled by their corresponding controllers, and V_o is indirectly regulated by summing all the module output voltages. According to the positive output voltage gradient regulation characteristics, for the controller of module 1, the module output voltage should be V_{o1A}, and the system output voltage should be V_{oA}, whereas for the controller of module 2, the module output voltage should be V_{o2B}, and the system output voltage should be V_{oB}. In practice, the real system output voltage is V_{oO}, and we can obtain $V_{oA} < V_{oO} < V_{oB}$. Therefore, for the controller of module 1, the system output voltage is considered to be higher than its corresponding reference voltage, and the duty cycle will be regulated to reduce the module output voltage V_{o1}, and the output power and the input power of module 1 are also reduced. Hence, the module input current $I_{\rm in1}$ will decrease, and I_{cd1} will increase; then, the input voltage of module 1 increases, and the working point moves up from point A. In the meantime,

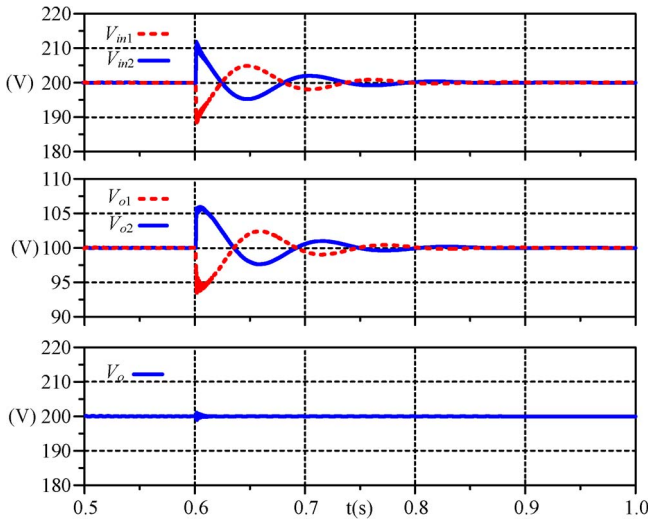

Fig. 7. Simulated individual input voltages, output voltages, and system output voltage corresponding to an input voltage perturbation.

for the controller of module 2, the system output voltage is considered to be lower than its corresponding reference voltage, and its duty cycle will be regulated to increase the module output voltage V_{o2}, and the output power and the input power of module 2 are also increased. Hence, $I_{\text{in}2}$ will increase, and I_{cd2} will decrease; then, the input voltage of module 2 decreases, and the working point moves down from point B. Finally, the operating points of the two modules return to the steady-state point O.

The operation principle is simulated for an ISOS system consisting of two converters, and the results are shown in Fig. 7. At steady state, the module input and output voltages are 200 and 100 V, respectively. At 0.6 s, an input voltage perturbation occurs, $V_{\text{in}1}$ decreases, and $V_{\text{in}2}$ increases. It can be seen that V_{o1} is reduced to shrink the output power and the input power of module 1 to raise $V_{\text{in}1}$; in the meantime, V_{o2} is increased to increase the output power and the input power of module 2 to decay $V_{\text{in}2}$, and finally, both input and output voltages converge to the steady point, and the system output voltage is almost undisturbed during the input voltage perturbation.

With the analysis and simulation, it can be seen that the constituent modules can evenly share the system input voltage with the proposed control strategy, and the output voltage sharing among the modules is automatically achieved. If the characteristics of the constituent modules are identical, the output voltage sharing is perfect.

In the foregoing analysis, the two modules evenly share the system input voltage with the assumption that the two modules have the same output voltage regulation characteristics as shown in Fig. 6; however, in practice, it is difficult to make the modules have exactly the same characteristics. The effect of the control parameters on the input voltage sharing accuracy will be analyzed with a two-module ISOS system. Assuming that the two modules have different voltage references, according to Fig. 5, at steady state, one can obtain

$$V_{\text{ref}1} + k_{\text{vi}} V_{\text{in}1} = k_{\text{vo}} V_o \tag{2}$$

$$V_{\text{ref}2} + k_{\text{vi}} V_{\text{in}2} = k_{\text{vo}} V_o. \tag{3}$$

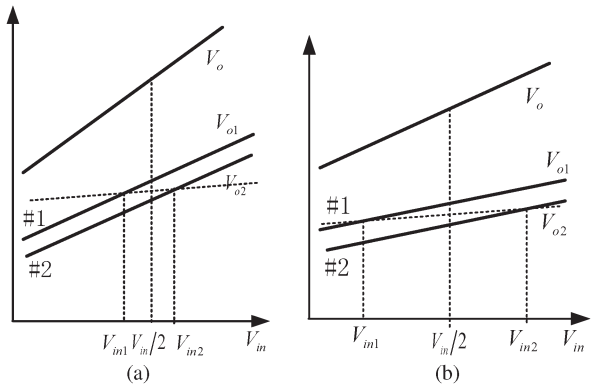

Fig. 8. Effect of k_{vi} on the input voltage-sharing accuracy and the system output voltage regulation. (a) Large k_{vi}. (b) Small k_{vi}.

Using (2) and (3), we have

$$V_{\text{ref}1} - V_{\text{ref}2} = k_{\text{vi}}(V_{\text{in}2} - V_{\text{in}1}) \tag{4}$$

$$V_o = \frac{V_{\text{ref}1} + V_{\text{ref}2} + k_{\text{vi}} V_{\text{in}}}{2k_{\text{vo}}} \tag{5}$$

$$\frac{\Delta V_o}{\Delta V_{\text{in}}} = \frac{V_{oa} - V_{ob}}{V_{\text{in}a} - V_{\text{in}b}} = \frac{\frac{V_{\text{ref}1}+V_{\text{ref}2}+k_{\text{vi}}V_{\text{in}a}}{2k_{\text{vo}}} - \frac{V_{\text{ref}1}+V_{\text{ref}2}+k_{\text{vi}}V_{\text{in}b}}{2k_{\text{vo}}}}{V_{\text{in}a} - V_{\text{in}b}} = \frac{k_{\text{vi}}}{2k_{\text{vo}}}. \tag{6}$$

From (4) and (6), it can be seen that, for a certain voltage reference deviation, the larger the k_{vi}, the better the input voltage-sharing accuracy; however, a larger k_{vi} leads to the deterioration of the system output voltage regulation performance. On the contrary, the smaller the k_{vi}, the worse the input voltage-sharing accuracy, but the system output voltage regulation performance is improved, as shown in Fig. 8. Moreover, the smaller the voltage reference mismatching, the better the input voltage-sharing accuracy. Therefore, a tradeoff must be made between the input voltage sharing and the output voltage regulation performance when designing the control circuit.

The proposed voltage-sharing control strategy is very similar to the droop method for the parallel operation of the dc–dc converters or dc–ac inverters to realize load current sharing [17]–[20]. In the droop method, the information of the module load current is introduced to each module's own controller to realize load current sharing. Correspondingly, in the proposed voltage-sharing control strategy, the information of the module input voltage is introduced to each module's own controller to realize input voltage sharing. The common advantage of the two control methods is that the current/voltage-sharing bus is eliminated, leading to superior system reliability and modularity. While the common shortage of the two control methods is the poor output voltage regulation performance, specifically, the droop method has the negative output voltage gradient regulation with the load current, whereas the proposed control strategy has the positive one. In order to improve the voltage

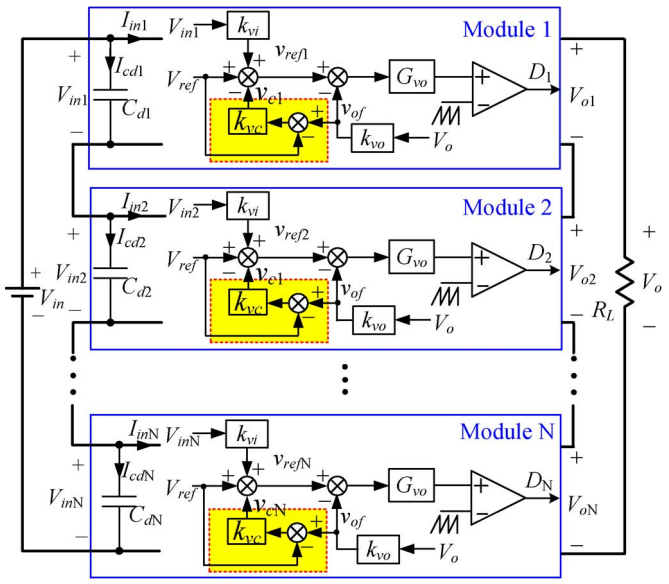

Fig. 9. Proposed decentralized voltage-sharing control strategy with improved output voltage regulation.

regulation of the droop method, a voltage shifting approach is proposed in [20]; although the voltage regulation performance is improved, an additional communication channel or current sharing bus is introduced to transmit the average current signal to each module, which cancels out the benefits of the droop method to some extent because the most important feature of the droop method is no control communication among the constituent modules.

In order to improve the voltage regulation of the ISOS system with respect to the input voltage variation, a novel voltage shifting approach is proposed in this paper without additional communication channel or voltage-sharing bus, as shown in the dashed lines in Fig. 9. In each module, the error signal between $v_{\rm of}$ and $V_{\rm ref}$ is amplified by k_{vc} times, and the output is subtracted from $V_{\rm ref}$. When $v_{\rm of}$ is higher than $V_{\rm ref}$, the output signal of the output voltage shifting loop v_{cj} $(j = 1, 2, \ldots, N)$ is positive, and this signal is subtracted from $V_{\rm ref}$, meaning that the real reference voltage of each module $v_{{\rm ref}j}$ $(j = 1, 2, \ldots, N)$ is decreased and the system output voltage will be decreased, correspondingly. v_{cj} $(j = 1, 2, \ldots, N)$ is identical due to that all the modules have the same $V_{\rm ref}$, $v_{\rm of}$, and k_{vc}, which means that same value is subtracted from $V_{\rm ref}$ for each module; hence, the introduction of the output voltage shifting loop has no influence on the operation principle of the proposed control strategy aforementioned.

According to Fig. 5, at steady state, we have $v_{\rm of} = v_{{\rm ref}j}$ $(j = 1, 2, \ldots, N)$, i.e.,

$$k_{\rm vo}V_o = V_{\rm ref} + k_{\rm vi}V_{{\rm in}j}, \qquad j = 1, 2, \ldots, N \tag{7}$$

$$V_{{\rm in}j} = \frac{V_{\rm in}}{N}, \qquad j = 1, 2, \ldots, N. \tag{8}$$

Combining (7) and (8), yields

$$V_o = \frac{1}{k_{\rm vo}}\left(V_{\rm ref} + k_{\rm vi}\frac{V_{\rm in}}{N}\right). \tag{9}$$

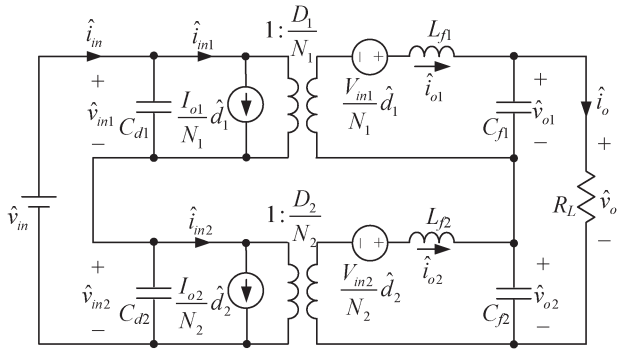

Fig. 10. Small-signal model of a two-module ISOS system.

TABLE I
SYSTEM PARAMETERS

Item	Symbol	Value
Filter inductance	L_f	200μH
Filter capacitance	C_f	2000μF
Input divided capacitance	C_{d1},C_{d2}	470μF
Output voltage	V_o	100V
Turns ratio	N	5/6
Gain of the ramp	F_m	1/2.5
Load resistance	R_L	20Ω
Input voltage sensing factor	K_{vi}	3/88
Duty cycle	D	0.4
Input voltage	V_{in}	200V

Hence, the gradient gain of the ISOS system without the output voltage shifting loop is

$$g_{s1} = \frac{k_{\rm vi}}{Nk_{\rm vo}}. \tag{10}$$

According to Fig. 9, at steady state, we have

$$k_{\rm vo}V_o = V_{\rm ref} + k_{\rm vi}V_{{\rm in}j} - k_{vc}(k_{\rm vo}V_o - V_{\rm ref}), \qquad j = 1, 2, \ldots, N \tag{11}$$

where k_{vc} is the gain of the output voltage shifting loop. Combining (8) and (11) yields

$$V_o = \frac{1}{k_{\rm vo} + k_{vc}k_{\rm vo}}\left(V_{\rm ref} + k_{\rm vi}\frac{V_{\rm in}}{N} + k_{vc}V_{\rm ref}\right). \tag{12}$$

Hence, the gradient gain of the ISOS system with the output voltage shifting loop is

$$g_{s2} = \frac{k_{\rm vi}}{Nk_{\rm vo}(1 + k_{vc})}. \tag{13}$$

According to (10) and (13), it can be seen that the gradient gain of the ISOS system can be significantly decreased with the output voltage shifting loop, leading to improved output voltage regulation performance. Moreover, with the output voltage shifting loop, a larger $k_{\rm vi}$ can be employed to ensure good input voltage-sharing accuracy. The concept of the proposed voltage shifting loop can be also applied to the droop method to improve the output voltage regulation without any additional communication channel or current sharing bus.

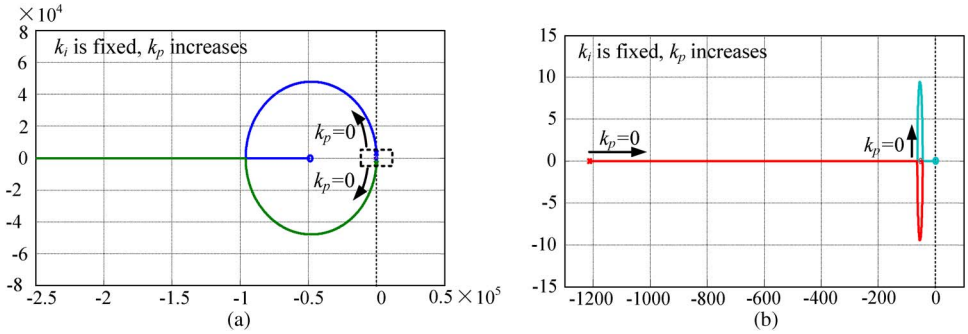

Fig. 11. (a) Root locus when $k_i = 1000$. (b) Expanded waveforms of the dashed box.

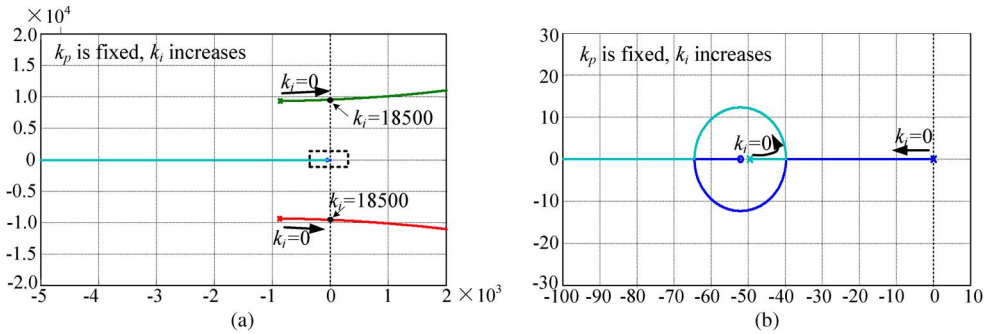

Fig. 12. (a) Root locus when $k_p = 10$. (b) Expanded waveforms of the dashed box.

IV. Stability Analysis of the Proposed Control Strategy

Here, the ISOS system stability with the proposed control strategy is studied. For simplicity, an ISOS system consisting of two forward converter modules is studied. The small-signal circuit model is shown in Fig. 10 [8], where $\hat{d}_1$ and $\hat{d}_2$ are the perturbations of the duty cycles; $\hat{v}_{\text{in}1}$ and $\hat{v}_{\text{in}2}$ are the perturbations of the individual input voltages; $\hat{i}_{o1}$ and $\hat{i}_{o2}$ are the perturbations of the individual output currents; N_1 and N_2 are the turns ratios of the transformers; and D_1, D_2, I_{o1}, and I_{o2} are the steady-state duty cycles and output currents, respectively.

For simplicity of analysis, the two converter modules are assumed to have the same turn ratio and the same output filter, i.e., $N_1 = N_2 = N$, $L_{f1} = L_{f2} = L_f$, and $C_{f1} = C_{f2} = C_f$. At steady state, $D_1 = D_2 = D$, we have

$$I_{o1} = I_{o2} = \frac{V_o}{R_L} \tag{14}$$

$$V_{\text{in}1} = V_{\text{in}2} = \frac{V_{\text{in}}}{2}. \tag{15}$$

According to Fig. 10, we obtain

$$\hat{i}_{o1} = \frac{N}{D}\left(\hat{i}_{\text{in}1} - \frac{V_o}{NR_L}\hat{d}_1\right) \tag{16}$$

$$\hat{i}_{o2} = \frac{N}{D}\left(\hat{i}_{\text{in}2} - \frac{V_o}{NR_L}\hat{d}_2\right) \tag{17}$$

$$\frac{D}{N}\hat{v}_{\text{in}1} + \frac{V_{\text{in}}}{2N}\hat{d}_1 = sL_f\hat{i}_{o1} + \hat{v}_{o1} \tag{18}$$

$$\frac{D}{N}\hat{v}_{\text{in}2} + \frac{V_{\text{in}}}{2N}\hat{d}_2 = sL_f\hat{i}_{o2} + \hat{v}_{o2} \tag{19}$$

$$\hat{v}_{o1} = \frac{1}{sC_f}\left(\hat{i}_{o1} - \frac{\hat{v}_o}{R_L}\right) \tag{20}$$

$$\hat{v}_{o2} = \frac{1}{sC_f}\left(\hat{i}_{o2} - \frac{\hat{v}_o}{R_L}\right). \tag{21}$$

According to Fig. 9, the perturbations of individual duty cycles can be expressed as follows:

$$\hat{d}_1 = G_{\text{vo}}F_m\left[k_{\text{vi}}\hat{v}_{\text{in}1} - k_{\text{vo}}(1+k_{vc})\hat{v}_o\right] \tag{22}$$

$$\hat{d}_2 = G_{\text{vo}}F_m\left[k_{\text{vi}}\hat{v}_{\text{in}2} - k_{\text{vo}}(1+k_{vc})\hat{v}_o\right] \tag{23}$$

where F_m is the gain of the ramp.

For the analysis of the input voltage sharing under condition of small-signal perturbation in total input voltage, the perturbation in the output voltage $\hat{v}_o$ can be neglected, assuming a fast output voltage controller and a large gain of the output voltage shifting loop [8], i.e.,

$$\hat{v}_o = 0. \tag{24}$$

Combining (16), (18), (20), (22), and (24) yields

$$Z_{\text{eq}1} = \frac{\hat{v}_{\text{in}1}}{\hat{i}_{\text{in}1}} = \frac{s^2L_fC_f+1}{G_{\text{vo}}F_mk_{\text{vi}}\frac{V_o}{NR_L}(s^2L_fC_f+1)+sC_f\frac{D}{N}\left(\frac{D}{N}+\frac{V_{\text{in}}}{2N}G_{\text{vo}}F_mk_{\text{vi}}\right)}. \tag{25}$$

Similarly, combining (17), (19), (21), (23), and (24) yields (26), shown at the bottom of the next page.

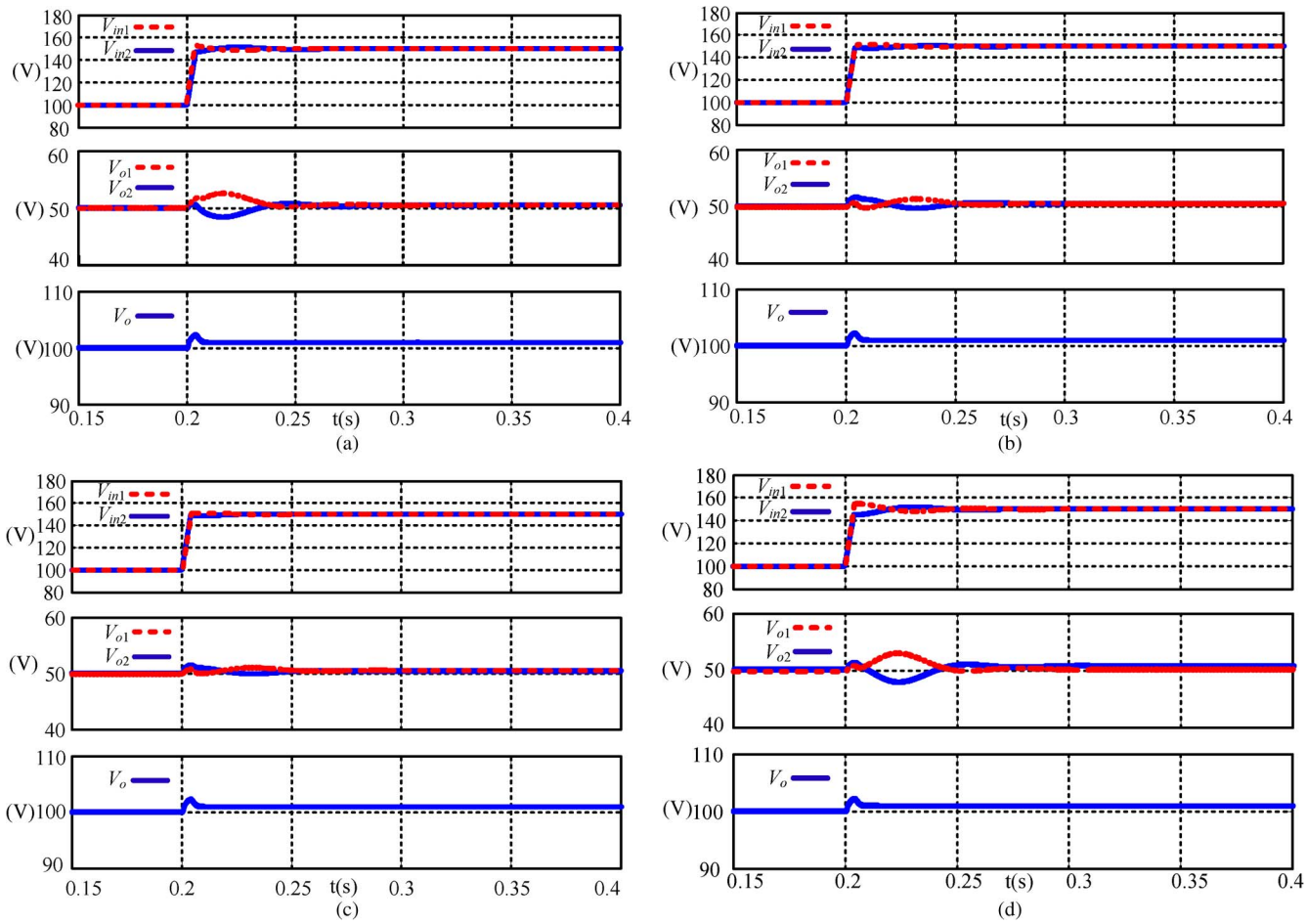

Fig. 13. Simulated individual input voltages, output voltages, and system output voltage corresponding to a stepped input voltage change in the case of component mismatch of modules 1 and 2. (a) Case of mismatch only in input divided capacitance ($C_{d1} = 400\ \mu$F, $C_{d2} = 470\ \mu$F). (b) Case of mismatch only in turns ratio($N_1 = 5/6.5, N_2 = 5/6$). (c) Case of mismatch only in filter inductance ($L_{f1} = 170\ \mu$H, $L_{f2} = 200\ \mu$H). (d) Case of mismatch in input divided capacitance, turns ratio, and filter inductance ($C_{d1} = 400\ \mu$F, $C_{d2} = 470\ \mu$F; $N_1 = 5/6.5$, $N_2 = 5/6$; $L_{f1} = 170\ \mu$H, $L_{f2} = 200\ \mu$H).

Hence, the input voltage difference between the two modules to the total input voltage can be expressed as

$$F(s) = \frac{\Delta\hat{v}_{\text{in12}}}{\hat{v}_{\text{in}}} = \frac{\hat{v}_{\text{in1}} - \hat{v}_{\text{in2}}}{\hat{v}_{\text{in}}} = \frac{sZ_{\text{eq}}(C_{d2} - C_{d1})}{2 + sZ_{\text{eq}}(C_{d2} + C_{d1})}. \tag{27}$$

For the output voltage loop, a classical proportional–integral (PI)-type regulator is used, and its transfer function G_{vo} can be expressed as

$$G_{\text{vo}} = k_p + \frac{k_i}{s}. \tag{28}$$

Substituting (25) and (28) into (27), the characteristic polynomial of $F(s)$ can be expressed as

$$D(s) = a_4 s^4 + a_3 s^3 + a_2 s^2 + a_1 s^1 + a_0 \tag{29}$$

where

$$\begin{cases} a_4 = L_f C_f (C_{d1} + C_{d2}) \\ a_3 = \frac{2V_o}{NR_L} L_f C_f F_m k_{\text{vi}} k_p \\ a_2 = \frac{2V_o}{NR_L} L_f C_f F_m k_{\text{vi}} k_i + 2C_f \frac{D^2}{N^2} \\ \quad + \frac{D}{N^2} C_f V_{\text{in}} F_m k_{\text{vi}} k_p + C_{d1} + C_{d2} \\ a_1 = \frac{D}{N^2} C_f V_{\text{in}} F_m k_{\text{vi}} k_i + \frac{2V_o}{NR_L} F_m k_{\text{vi}} k_p \\ a_0 = \frac{2V_o}{NR_L} F_m k_{\text{vi}} k_i. \end{cases} \tag{30}$$

As shown in (30), the polynomial has all positive coefficients; however, for the system to be stable, the following has to be satisfied:

$$b_1 = \frac{a_2 a_3 - a_1 a_4}{a_3} > 0 \tag{31a}$$

$$b_2 = \frac{(a_2 a_3 - a_1 a_4) a_1 - a_3^2 a_0}{a_2 a_3 - a_1 a_4} > 0. \tag{31b}$$

$$Z_{\text{eq2}} = \frac{\hat{v}_{\text{in2}}}{\hat{i}_{\text{in2}}} = \frac{s^2 L_f C_f + 1}{G_{\text{vo}} F_m k_{\text{vi}} \frac{V_o}{NR_L} (s^2 L_f C_f + 1) + sC_f \frac{D}{N} \left(\frac{D}{N} + \frac{V_{\text{in}}}{2N} G_{\text{vo}} F_m k_{\text{vi}} \right)} = Z_{\text{eq1}} = Z_{\text{eq}} \tag{26}$$

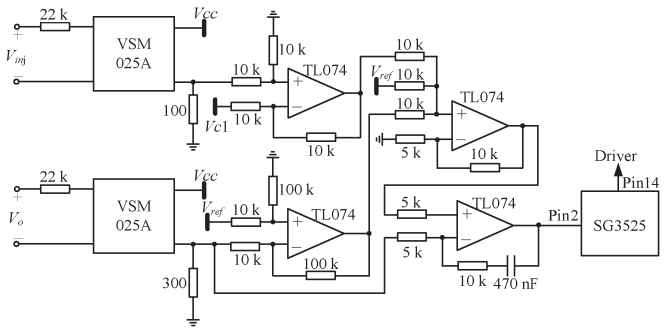

Fig. 14. Electrical diagram of the control circuit for the proposed control strategy.

With proper selection of different k_p and k_i, (31) can be satisfied, and the system will be stable. Selection guidance is based on root locus analysis, and the system parameters are listed in Table I.

The closed-loop root locus for different k_p is shown in Fig. 11. The value of k_i is fixed to be 1000, whereas the value of k_p increases from zero to test the system stability. The dashed box shown in Fig. 11(a) is expanded in Fig. 11(b). It can be seen that the system is always stable for different k_p.

The closed-loop root locus for different k_i is shown in Fig. 12. The value of k_p is fixed to be 10, whereas the value of k_i increases from zero to test the system stability. The dashed box shown in Fig. 12(a) is expanded in Fig. 12(b). As shown in Fig. 12, the system goes from stable to unstable when the value of k_i reaches 18 500 since the roots go from the left-half plane to the right-half plane. Hence, it is concluded that the ISOS system with the proposed decentralized voltage-sharing control strategy is stable if the PI parameters of the voltage compensator are properly selected.

In order to verify the system stability of the proposed method even in the case of large variations in component values, an ISOS system consisting of two forward converters is built for simulation. The basic system parameters are listed in Table I. Four cases of component mismatch are simulated, i.e., mismatch in input divided capacitance, mismatch in turns ratio of the power transformer, mismatch in output filter inductance, and mismatch in all of the above three items, respectively [21]. The simulation waveforms of individual input voltages, output voltages, and system output voltage corresponding to a stepped input voltage change from 200 to 300 V in the case of components mismatch are shown in Fig. 13. It can be seen that the large variations in component values have no influence on the system stability and the input voltage sharing.

V. Experimental Results

In order to verify the feasibility of the proposed control strategy, an ISOS system consisting of three two-transistor forward converter modules has been built in the laboratory, and the specifications are listed as follows:

- system input voltage V_{in}: 300–450 V;
- system output voltage V_o: 150 V;
- maximum output current I_o: 5 A.

For each module, the input voltage is 100–150 V, the output voltage is 50 V, and the maximum output power is 250 W.

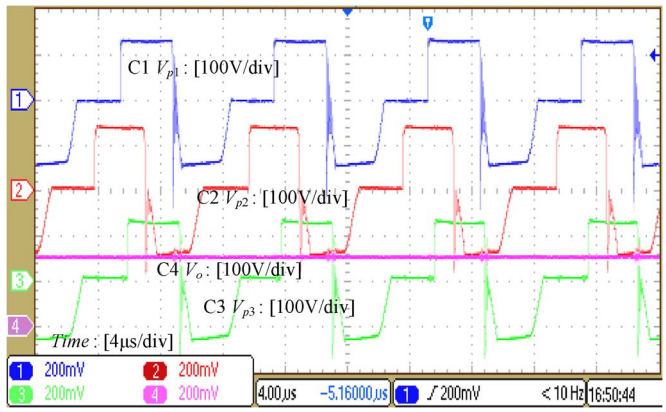

Fig. 15. Voltages across the primary windings of individual transformers under steady state.

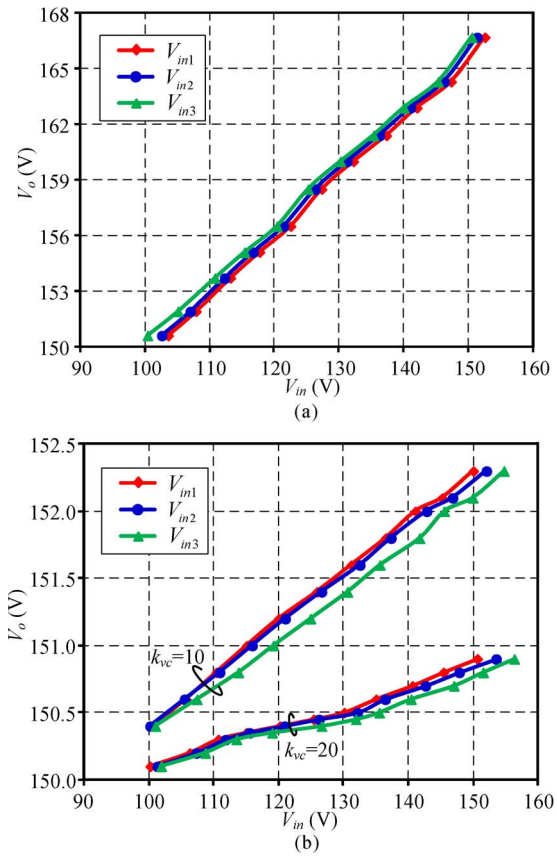

Fig. 16. Measured output voltage regulation curves of three modules. (a) Without voltage shifting loop. (b) With voltage shifting loop.

The detailed control diagram block of the proposed control strategy is shown in Fig. 14. VSM025A is a voltage transducer based on the measuring principle of the Hall effect with a galvanic isolation between the module input voltage and the system output voltage. V_{cc} is the power supply of the control circuit. In Fig. 14, V_{c1} is subtracted from the sampled signal of the module input voltage, which is not illustrated in Figs. 5 and 9; V_{c1} is equal to the sampled value of the module minimum input voltage. Therefore, the real value added to V_{ref} is zero under minimum input voltage.

It should be noted that V_{c1} can be also set as the sampled value of a certain constant value between the module minimum

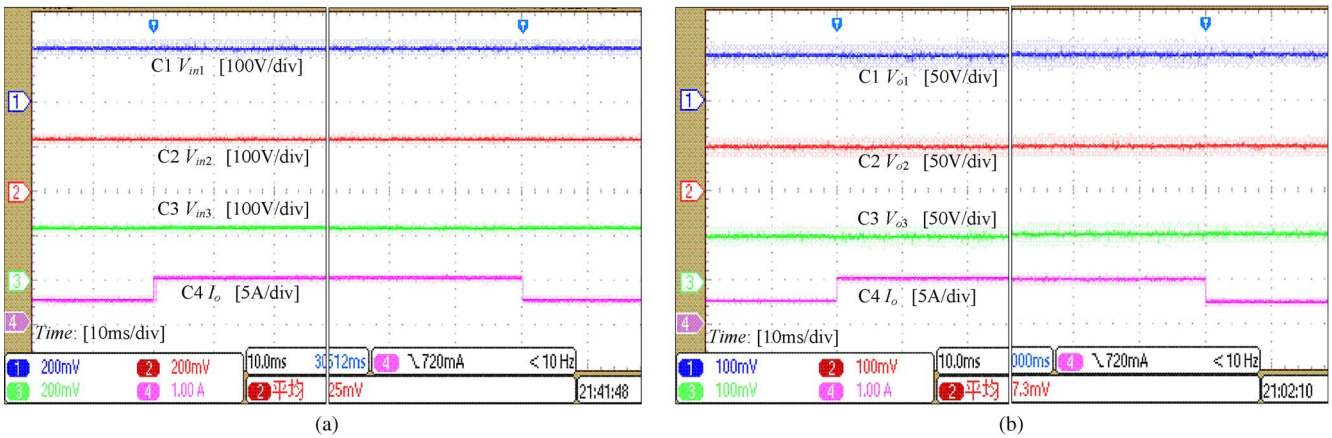

(a) (b)

Fig. 17. Experimental waveforms in case of stepped load. (a) Individual input voltages and output current. (b) Individual output voltages and output current.

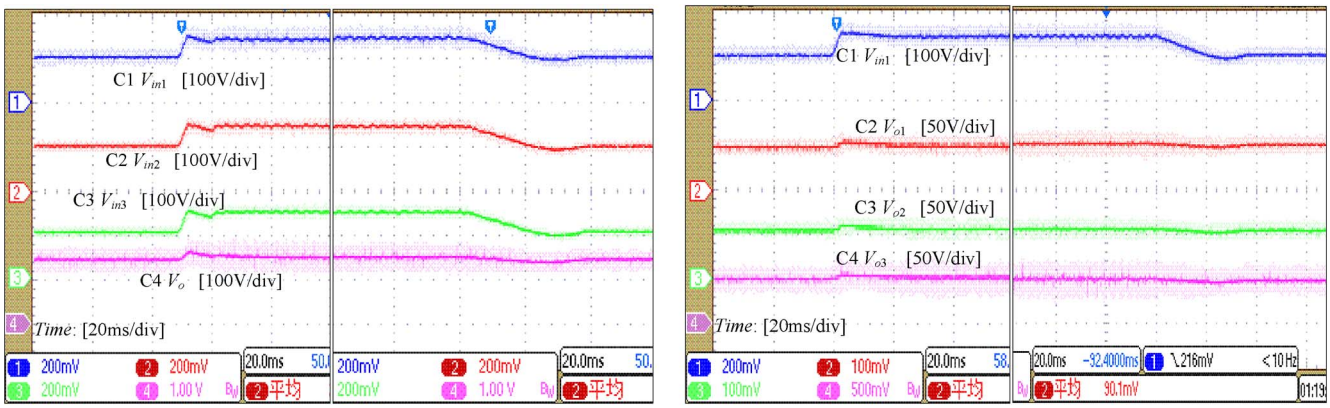

(a) (b)

Fig. 18. Experimental waveforms in case of stepped input voltage. (a) Individual input voltages and system output voltage. (b) Individual output voltages and input voltage of module 1.

input voltage and maximum input voltage. For example, V_{c1} can be also equal to the sampled value of $V_{\text{in nom}}/N$, where $V_{\text{in nom}}$ is the center of the input voltage range.

Fig. 15 shows the voltages across the primary winds of individual transformers under normal input voltage (400 V) and full load. It can be seen that all the voltages have almost the same positive amplitudes, which means that the module input voltages are equal.

Fig. 16 shows the measured curves of the system output voltage regulation when the ISOS system input voltage varies from 300 to 450 V. Fig. 16(a) shows the measured curves without the voltage shifting loop (refer to Fig. 5); it can be seen that the increase in the system output voltage (ΔV_o) is nearly 17 V in the whole system input voltage range and that the input voltages of the three modules are well shared. Fig. 16(b) shows the measured curves with the voltage shifting loop (refer to Fig. 9) when $k_{vc} = 10$ and 20. As shown, ΔV_o is significantly reduced with the introduction of the voltage shifting loop, and $\Delta V_o = 0.8$ V when $k_{vc} = 20$, which means that the system output voltage regulation is 0.53% with respect to input voltage variation (300–450 V). Due to small mismatches in the controller parameters among the three prototypes, such as reference voltages, voltage sensors, and operational amplifiers, the measured maximum input voltage difference among the three modules is 5 Vdc, which is acceptable.

Figs. 17 and 18 show the experimental waveforms of the ISOS system corresponding to stepped load and stepped input voltage, respectively. Fig. 17 shows the input voltages and the output voltages of the three modules corresponding to a load stepping between half-load (2.5 A) and full-load (5 A) when system input voltage is 400 V. Fig. 18 shows the input voltages and the output voltages of the three modules and the system's output voltage corresponding to an input voltage stepping between 300 and 450 V under full-load condition. It can be seen that input voltages are well shared both at steady state and during transient, and sharing of the output voltage is automatically achieved.

In order to verify the redundancy of the ISOS system with the proposed decentralized control strategy, a fault is imitated in the ISOS system prototype by shorting the input capacitor of module 1 with a switch in series with a 0.5-Ω resistor limiting the discharging current of the capacitor, and a diode is antiparalleled with its filter capacitor to freewheel the load current. Fig. 19 shows the experimental waveforms in case of module 1 is isolated (closing the short switch) and inserted (opening the short switch) under system input voltage $V_{\text{in}} =$ 330 V and full-load condition, respectively. After opening the short switch, the input capacitor of module 1 is charged by the system input current, and the module input/output voltage increases; in the meantime, the input/output voltages of

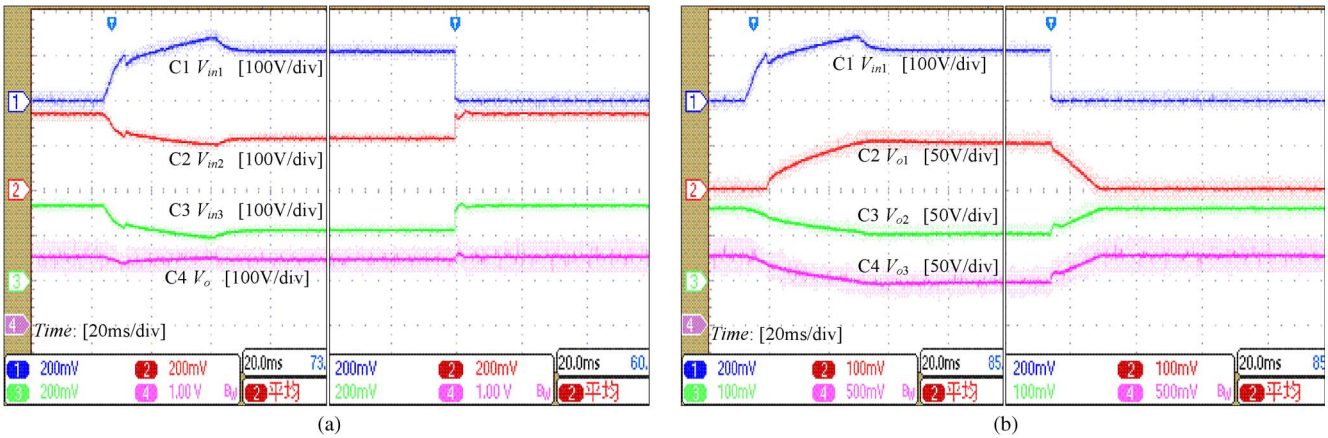

(a) (b)

Fig. 19. Experimental waveforms in case of module 1 is inserted and isolated, respectively. (a) Individual input voltages and system output voltage. (b) Individual output voltages and input voltage of module 1.

modules 2 and 3 decrease. After a certain amount of regulation time, the three modules share the system input voltage, and the system output voltage is recovered to be stable. When the short switch is closed, the system input voltage is still evenly shared by the remaining two modules. The output voltage of module 1, i.e., V_{o1}, slowly decreases due to the energy stored in its filter capacitor, and in the meantime, the output voltages of modules 2 and 3, i.e., V_{o2} and V_{o3}, increase correspondingly. In addition, it should be noted that the corner present in the Fig. 19 is actually caused by the integrator windup. It can be seen that, without any control interconnection among the modules, redundancy in combination with hot-swap capability of modules can be easily achieved.

VI. Conclusion

This paper has proposed a decentralized voltage-sharing method for the ISOS connection of dc–dc converters to realize fully modular design. Its main feature is that it does not require any control communication link among the constituent modules. The proposed voltage sharing method uses the positive output voltage gradient regulation of the series modules to achieve an even distribution of the input/output voltages among them. Moreover, a voltage shifting loop is introduced to improve the system output voltage regulation. The decentralized voltage-sharing method has the following advantages: 1) all the modules have the same power stages and control stages, which facilitates the system design; 2) control circuits are distributed into each module, and there is no central controller; and 3) the system modularity, reliability, and maintainability are improved. Experimental results of a three-module ISOS system verify the effectiveness of the proposed control strategy.

References

[1] I. Baraia, J. Barrena, G. Abad, J. Segade, and U. Iraola, "An experimentally verified active gate control method for the series connection of IGBT/diodes," *IEEE Trans. Power Electron.*, vol. 27, no. 2, pp. 1025–1038, Feb. 2012.

[2] S. Inoue and H. Akagi, "A bidirectional isolated dc–dc converter as a core circuit of the next-generation medium-voltage power conversion system," *IEEE Trans. Power Electron.*, vol. 22, no. 2, pp. 535–542, Mar. 2007.

[3] B. R. Lin and C. Chao, "Soft-switching converter with two series half-bridge legs to reduce voltage stress of active switches," *IEEE Trans. Ind. Electron.*, vol. 60, no. 6, pp. 2214–2224, Jun. 2013.

[4] W. Chen, X. Ruan, H. Yan, and C. Tse, "DC/DC conversion systems consisting of multiple converter modules: Stability, control and experimental verifications," *IEEE Trans. Power Electron.*, vol. 24, no. 6, pp. 1463–1474, Jun. 2009.

[5] R.-L. Lin, W.-S. Liu, J.-F. Chen, M.-H. Chen, and C.-H. Liu, "Positive feedforward control for multimodule output-series power-conversion systems with individual nonideal sources," *IEEE Trans. Ind. Electron.*, vol. 60, no. 4, pp. 1323–1340, Apr. 2013.

[6] Y. Hayashi, "Approach for highly efficient and ultra compact converters in next generation 380 V dc distribution system," in *Proc. IEEE ECCE*, 2012, pp. 3803–3810.

[7] C. Zhan, A. Bullock, C. Smith, and A. Crane, "Power collection and transmission systems," EP Patent 2 341 594 A1, Jul. 6, 2011.

[8] R. Giri, V. Choudhary, R. Ayyanar, and N. Mohan, "Common-duty-ratio control of input-series connected modular dc–dc converters with active input voltage and load-current sharing," *IEEE Trans. Ind. Appl.*, vol. 42, no. 4, pp. 1101–1111, Jul./Aug. 2006.

[9] P. J. Grbović, "Master/slave control of input-series-and output-parallel-connected converters: Concept for low-cost high-voltage auxiliary power supplies," *IEEE Trans. Power Electron.*, vol. 24, no. 2, pp. 316–328, Feb. 2009.

[10] X. Ruan, "Control strategy for input-series–output-parallel converters," *IEEE Trans. Ind. Electron.*, vol. 56, no. 4, pp. 1174–1185, Apr. 2009.

[11] D. Sha, Z. Guo, and X. Liao, "Cross-feedback output-current-sharing control for input-series–output-parallel modular dc–dc converters," *IEEE Trans. Power Electron.*, vol. 25, no. 11, pp. 2762–2771, Nov. 2010.

[12] D. Sha, K. Deng, Z. Guo, and X. Liao, "Control strategy for input-series–output-parallel high-frequency ac link inverters," *IEEE Trans. Ind. Electron.*, vol. 59, no. 11, pp. 4101–4111, Nov. 2012.

[13] R. Giri, R. Ayyanar, and E. Ledezma, "Input-series and output-series connected modular dc–dc converters with active input voltage and output voltage sharing," in *Proc. IEEE APEC Expo.*, 2004, pp. 1751–1754.

[14] Q. Lu, Z. Yang, S. Lin, S. Wang, and C. Wang, "Research on voltage sharing for input-series–output-series phase-shift full-bridge converters with common-duty-ratio," in *Proc. IEEE IECON*, 2011, pp. 1548–1553.

[15] J. Merwe and H. Mouton, "An investigation of the natural balancing mechanisms of modular input-series–output-series dc–dc converters," in *Proc. IEEE ECCE*, 2010, pp. 817–822.

[16] D. Sha, K. Deng, and X. Liao, "Duty cycle exchanging control for input-series–output-series connected two PS-FB dc–dc converters," *IEEE Trans. Power Electron.*, vol. 27, no. 3, pp. 1490–1501, Mar. 2012.

[17] J. W. Kim, H. S. Choi, and B. H. Cho, "A novel droop method for converter parallel operation," *IEEE Trans. Power Electron.*, vol. 17, no. 1, pp. 25–32, Jan. 2002.

[18] Q.-C. Zhong, "Robust droop controller for accurate proportional load sharing among inverters operated in parallel," *IEEE Trans. Ind. Electron.*, vol. 60, no. 4, pp. 1281–1290, Apr. 2013.

[19] X. Lu, K. Sun, J. M. Guerrero, J. C. Vasquez, and L. Huang, "State-of-charge balance using adaptive droop control for distributed energy storage systems in dc microgrid applications," *IEEE Trans. Ind. Electron.*, vol. 61, no. 6, pp. 2804–2815, Jun. 2014.
[20] S. Anand, B. G. Fernandes, and J. M. Guerrero, "Distributed control to ensure proportional load sharing and improve voltage regulation in low-voltage dc microgrids," *IEEE Trans. Power Electron.*, vol. 28, no. 4, pp. 1900–1912, Apr. 2013.
[21] J. W. Kimball, J. T. Mossoba, and P. T. Krein, "A stabilizing, high-performance controller for input series-output parallel converters," *IEEE Trans. Power Electron.*, vol. 23, no. 3, pp. 1416–1427, May 2008.

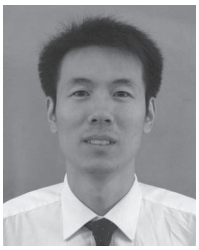

Wu Chen (S'05–M'12) was born in Jiangsu, China, in 1981. He received the B.S., M.S., and Ph.D. degrees from Nanjing University of Aeronautics and Astronautics, Nanjing, China, in 2003, 2006, and 2009, respectively, all in electrical engineering.

From 2009 to 2010, he was a Senior Research Assistant with the Department of Electronic Engineering, City University of Hong Kong, Kowloon, Hong Kong. In 2010–2011, he was a Postdoctoral Researcher with the Future Electric Energy Delivery and Management Systems Center, North Carolina State University, Raleigh, NC, USA. Since September 2011, he has been an Associate Research Fellow with the School of Electrical Engineering, Southeast University, Nanjing. His main research interests include soft-switching converters, microgrid, and power electronic system integration.

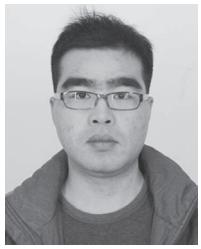

Guangjiang Wang was born in Henan Province, China, in 1989. He received the Bachelor's degree in electrical engineering from Henan University of Technology, Zhengzhou, China, in 2012. He is currently working toward the Master's degree in electrical engineering in the School of Electrical Engineering, Southeast University, Nanjing, China.

His current research interests include power electronics technology and applications of power electronics in power systems.